

STP 1638, 2022 / available online at [www.astm.org](http://www.astm.org) / doi: 10.1520/STP163820210045

Akshat Agha<sup>1</sup> and Fadi Abu-Farha<sup>1</sup>

# Advanced Anti-Buckling Device Coupled with Real-Time Digital Image Correlation for Complex Cyclic Tension-Compression Testing of Lightweight Materials

## Citation

A. Agha and F. Abu-Farha, "Advanced Anti-Buckling Device Coupled with Real-Time Digital Image Correlation for Complex Cyclic Tension-Compression Testing of Lightweight Materials," in *Evaluation of Existing and New Sensor Technologies for Fatigue, Fracture, and Mechanical Testing*, ed. J. Kang, P. C. McKeighan, G. Dahlberg, and R. Kemmerer (West Conshohocken, PA: ASTM International, 2022), 40-54. <http://doi.org/10.1520/STP163820210045><sup>2</sup>

## ABSTRACT

In sheet metal forming and stamping operations, modeling the behavior of sheet metal alloys for springback prediction is known to be very challenging, not only because of the complex models needed to account for kinematic hardening (such as the Yoshida-Uemori Model) but more importantly because of the experimental limitations of our ability to perform the complex tests needed to calibrate such models. For instance, reliable monotonic uniaxial compression tests and then cyclic tension-followed-by-compression tests are essential for characterizing the response of the material under those loading conditions, providing quantitative evaluation of the Bauschinger effect and tension-compression asymmetry in the material, and ultimately generating the right data to calibrate the constitutive model. This work tries to shed some light on this topic by introducing a new antibuckling device that is particularly designed to enable accurate and repeatable compression and cyclic testing. The device exerts side loading on the sheet test sample to prevent it from buckling during

---

Manuscript received May 11, 2021; accepted for publication June 11, 2021.

<sup>1</sup>FADI-AMT LLC, 48 Brookfield Oaks Dr., Suite D, Greenville, SC, 29607, USA A. A.  <https://orcid.org/0000-0001-9992-1114>

<sup>2</sup>ASTM Fifth Symposium on *Evaluation of Existing and New Sensor Technologies for Fatigue, Fracture, and Mechanical Testing* held virtually on May 19–20, 2021.

testing under compression loading conditions. The device is designed to address the limitations of other approaches and devices presented in the literature, and it features control and monitoring of side forces, self-centering, and the ability to achieve large plastic compressive strains. More importantly, digital image correlation (DIC) is integrated with the antibuckling device and testing load frame to provide accurate strain measurements. In this study, DIC was used in a real-time mode (unlike the typical postdeformation mode) to facilitate accurate load reversal during cyclic testing. For validation, the presented setup was used for testing two selected materials with practical applications in the automotive body sector: AA6016-T4 and DP980 steel sheets. The results demonstrate how the developed setup and the integration with real-time DIC provide a robust and reliable means for generating high-quality curves for the different tests needed for the calibration of springback models.

### Keywords

antibuckling device, cyclic testing, tension-compression test, springback, Yoshida-Uemori Model, digital image correlation, real-time strain control

## Introduction

In recent years, the drive to design and manufacture energy-efficient vehicles has propelled the automotive industry toward lightweighting with advanced materials, including high-strength aluminum alloys and advanced high-strength steels (AHSS) exhibiting high strength and ductility. However, several undesirable phenomena are associated with the forming of such materials; prominent and complex springback response is among the most critical of them. Springback magnitude is directly proportional to the ratio of flow stresses to Young's modulus; this makes it typically high for such high-strength materials. More importantly, the strong anisotropy of aluminum alloys and the multiphase microstructures of AHSS result in tension-compression asymmetry, leading to complex springback behaviors and therefore necessitating the development of complex predictive models.

Several efforts in the literature have tried to understand the springback behavior of sheet metal alloys. During stamping, materials are known to experience loading and unloading cycles, as well as to switch between tension and compression loading cases. Cold working in a material increases its tensile yield strength but has a negative impact on the compressive yield strength due to the Bauschinger effect.<sup>1,2</sup> When the material is unloaded after being loaded plastically, the stress-strain response, particularly for high-strength steels, is nonlinear. Upon reloading, the material shows a nonlinear elastic response that is different from the unstrained material. The elastic modulus decreases with the increase in plastic strain, a phenomenon known as modulus decay.<sup>3-5</sup> These complex phenomena make it more challenging to model the springback behavior of lightweight metals. Predictive springback models in the literature are generally dependent on four types of material response and thus require four corresponding types of physical mechanical

tests: (1) uniaxial tension tests, (2) tension load-unload (LU) tests, (3) uniaxial compression tests, and (4) tension-compression (TC) cyclic tests.

Notable works by Yoshida and Uemori,<sup>6–7</sup> Ghaei et al.,<sup>3</sup> Lee et al.,<sup>5</sup> Sun and Wagoner,<sup>8</sup> and Chongthairungruang<sup>9</sup> discuss the modeling of springback using cyclic TC and LU curves. The use of cyclic TC data and uniaxial tension LU data is not limited to springback prediction but is also extended to other forming applications, such as single-point incremental forming of sheet metals.<sup>10</sup> Although there have been improvements in the theoretical modeling, material characterization techniques still lag in terms of the ability to produce reliable data, simply due to the complex nature of these tests. Various experimental techniques have been tried to determine the material properties of sheet metals along cyclic loading paths. It is still possible to measure small compressive strains on round specimens with appropriate length-to-diameter ratios;<sup>11</sup> however, large strains under in-plane compression testing of sheet metals are not easy to obtain due to the material's tendency to buckle under compressive loading. Various methods and devices have been proposed in the literature to suppress the out-of-plane buckling while testing. Yoshida et al.<sup>12</sup> tested a laminated specimen consisting of multiple sheet metal dog bone specimens bonded by an adhesive to overcome buckling in a single specimen. The study was performed on a mild steel (SPCC) and a high-strength steel (SPFC), and a maximum cyclic strain of ~8% was obtained. Yoshida et al. successfully used this approach to generate full-cycle TC loops. While the results are encouraging, the approach may not be practical. Yoshida et al. used a clip-on extensometer for strain measurements. Boger et al.<sup>13</sup> used solid flat plates as buckling constraints and applied normal side force on the test specimen using a hydraulic clamping system. The side force was controlled but not recorded. The setup was used successfully for compressive testing of prestrained tension samples, achieving compressive recovery strains of ~18% for AA6022 and Mg AZ31B, but without using any extensometers due to setup limitations. Full loops of cyclic tests were done using optical extensometers but to a small cyclic strain of 2%. Kuwabara et al.<sup>14</sup> proposed a new setup where two comb-type dies were used to support the sheet specimen during testing and thus prevent it from buckling. Compressive strains of up to ~6% were achieved in monotonic compression testing for both phosphor bronze and AA6016-T4 sheets. Cyclic testing was performed; however, the maximum strain limit in a single loop cyclic test was ~1.5%. While this approach produced good results for the two mentioned materials, the test specimen was still prone to buckle in between each pair of teeth of the die. No details were provided regarding the method used for strain measurements. Li et al.,<sup>15</sup> on the other hand, also proposed a setup with two comb-type dies to support the test specimen; however, the setup relied on eight bolts for changing the amount of side force exerted on the specimen. While this was an improvement over the work of Kuwabara et al., the side force was still not easy to control. Real-time side force was recorded for friction force corrections. Strain measurements were done using an optical noncontact extensometer;

however, the latter was tracking test specimen deformation through two slotted holes in the clamping plate. Full-single-loop cyclic TC testing was performed on B170P1 and DP590 steel sheets, and a maximum compressive strain of  $\sim 6\%$  was achieved. Cao et al.<sup>16</sup> developed a double-wedge setup to provide side force and prevent buckling in the specimen, yet the side force was achieved by six screws and thus did not allow quantification or control of the side force during testing. Moreover, two fins had to be extended from each test specimen to enable strain monitoring by a laser extensometer. The setup was used to test BH180, DP600 steel, and AA6111-T4 sheets to achieve monotonic compressive strains up to  $\sim 10\%$ ; no full-loop cyclic TC testing (single or multiple loops) was reported.

Overall, the fixtures and devices presented in the literature had good features, but they were not comprehensive enough to cover all the issues encountered in this type of complex testing. Except for the work of Boger et al., none of the devices had a reliable control over the side force. Most of the works used either no extensometer or a clip-on extensometer. The attempts with noncontact extensometers were limited to low compressive strains. Therefore, none of the presented systems used easy and reliable strain measurement techniques, particularly capitalizing on the latest developments in noncontact strain measurements via digital image correlation (DIC). DIC is critical because we have no information on the degree of uniformity of the strains developed in the material specimen during testing, and only DIC can reveal that. Few efforts showed testing of AHSS; none tested any AHSS of  $\sim 1.0$  GPa tensile strength or higher. Finally, none showed high-quality multiloop TC cyclic curves for a good array of materials.

In the present study, a novel antibuckling device for controlled and reliable sheet specimen support is introduced; the device addresses most of the open issues encountered in monotonic compression testing as well as cyclic TC testing. The device is capable of controlling and recording the side forces on the specimen throughout the test for friction and biaxial corrections in the test results. The device has an auto-alignment feature that can adapt to sheet specimens of any thickness. Moreover, the device is integrated with DIC for full-field strain measurements within the test specimen. The DIC is not used in the conventional postdeformation mode; rather, it records the strains on the surface of the specimen in real-time mode, which provides direct feedback to the testing system to enable precise strain reversal. The paper first explains the details of the antibuckling device and its integration with DIC, highlighting the features incorporated in order to resolve the prominent issues in this field of testing. Two materials are then considered: AA6016-T4 aluminum alloy and DP980 steel sheets; the materials represent high-strength grades of aluminum and steel with important automotive body applications. The developed setup is used to test the two materials covering the uniaxial tension, tension LU, uniaxial compression, and cyclic TC tests. Results are then presented; they highlight the ability to obtain high-quality stress-strain curves for high strains and multiple cyclic loops (for accurate calibration of the most complex kinematic hardening springback models), as well as the

enrichment brought about by DIC in revealing the levels of deformation homogeneity that can be expected from such tests.

## Materials and Methods

### TEST SETUP

The core of the developed setup is the antibuckling device, which is designed to fit any quasi-static load frame. In this study, the device was fitted on a ZwickRoell Z2020 electro-mechanical load frame equipped with a 20-kN load cell for axial load measurements. The antibuckling device is shown in [figure 1](#); it is simply a rigid cage structure containing a drive train featuring an air cylinder and a load cell, as well as two contact blocks (plates) that sandwich a test specimen within the gauge region. When the air cylinder is engaged via an external flow valve, the two plates apply a firm side force that can be accurately controlled (by the amount of applied air pressure) and also monitored and corrected via the side load cell. In addition, the whole cage assembly can slide freely in the horizontal direction to allow self-centering of the device. The flexible nature of this mechanism allows for enough space to mount and remove the test specimen during setup while accommodating sheet specimens of practically any thickness during testing. The test specimen is mounted to the load frame via two custom grips that can withstand pulling and pushing forces up to  $\sim$ 20 kN. To reduce the effects of friction induced by the antibuckling contact blocks, a lubricant is used between them and the test specimen.

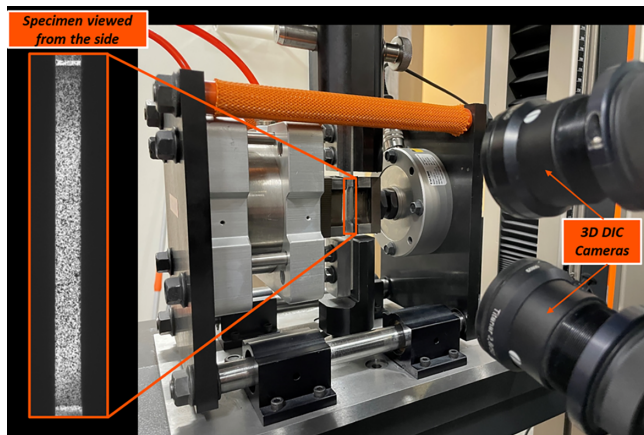
### Real-Time DIC System

The main highlight of the setup was the integration of three-dimensional (3D) DIC with the antibuckling device and the load frame. As shown in [figure 2](#), DIC cameras

**FIG. 1** Antibuckling device mounted onto a universal load frame.



**FIG. 2** 3D DIC in real-time mode live-tracking the deformation on the side of the specimen.



were set up for viewing the test specimen from the side (the free surface of the specimen, since the gauge region surfaces were under compression from the anti-buckling plates). The GOM ARAMIS 12M 3D DIC system with high-resolution cameras was used, achieving a measurement pixel density of less than  $9 \mu\text{m}$  per pixel. The specimens were speckle-patterned on their sides, and the DIC system was set for tracking the axial strain along a 16-mm-long virtual extensometer. For the monotonic tension and compression tests, DIC was used in the conventional mode. For the cyclic TC tests as well as the tension LU tests, the DIC system was operated in a real-time control mode and by feeding the live strains into the load frame; custom cyclic loading programs were prepared, and the live DIC strains were used to accurately reverse the direction of loading at the exact points of interest.

## MATERIALS

Two materials were selected for testing: 1.2-mm-thick DP980 steel sheets and 2.5-mm-thick AA6016-T4 sheets. The general relevant mechanical properties of these two materials are given in [table 1](#). Test specimens were cut out of the sheets by

**TABLE 1** Mechanical properties of the DP980 and AA6016-T4 sheets tested in this study

Material	Yield Strength, MPa	Tensile Strength, MPa	Total Ductility, %
DP980	790	1056	16
AA6016-T4	165	275	32

wire-cut electrical discharge machining (Wire-EDM) per a custom geometry specifically suited for compression and cyclic testing; the same geometry was used for all tests, including tension tests and LU tests to maintain consistency. The test specimens had a gauge region of 20 mm × 10 mm; while this is a low length-to-width ratio, it is necessary for this type of testing to assist in mitigating certain modes of buckling.

## Experimental Results and Analysis

### TESTING CONDITIONS

All the mechanical tests performed in this study were carried out at an ambient temperature and a quasi-static strain rate of  $\sim 0.002\text{ s}^{-1}$  (axial pulling or compressive deformation). In the transverse direction, and for those tests that required the use of the antibuckling device, a side force of 2 kN was determined to be sufficient for the AA6016-T4 samples, while a higher side force of 4 kN was used with the DP980 samples. DIC images were captured at a fixed frame rate of 20 Hz. Captured images were processed by GOM Correlate Professional DIC software.

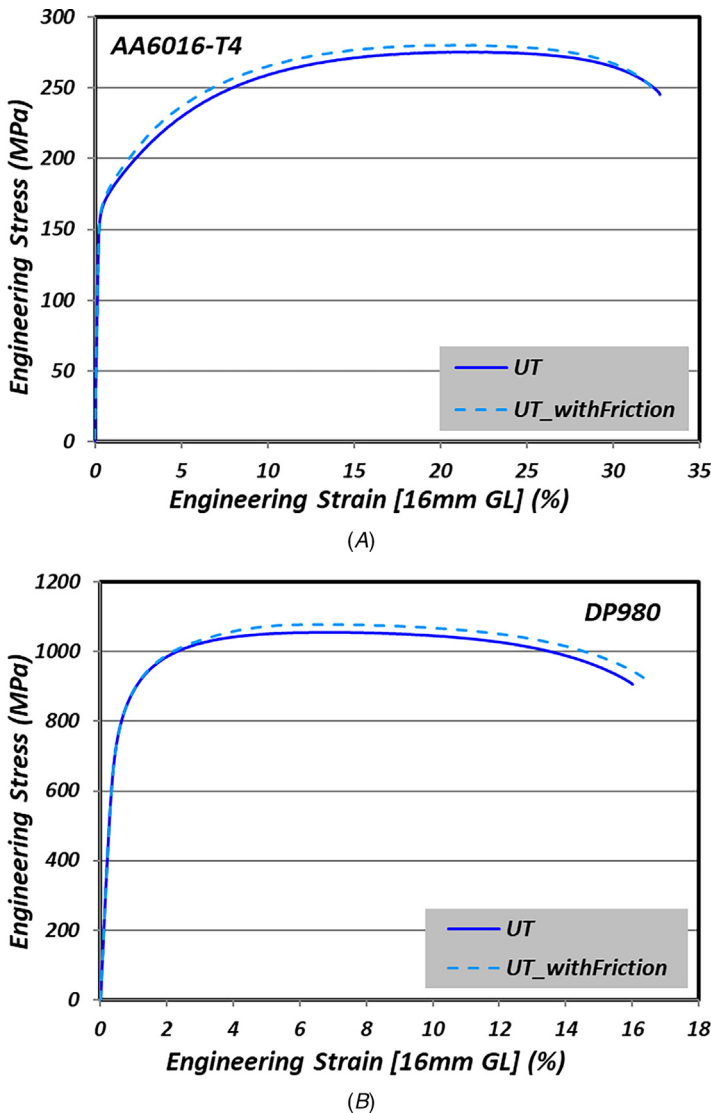
### UNIAXIAL TENSION TESTS

The uniaxial tension tests were first performed to establish the baseline behavior of each material. An antibuckling device is obviously not needed for tension testing; nevertheless, testing was carried out in two ways: (1) without side force (antibuckling plates fully open), and (2) with side force from the antibuckling device, and with the same level of forces used in subsequent compression and TC tests. The difference in force levels between the two scenarios was used to evaluate the friction forces from the contact blocks of the antibuckling device, and that correction factor was used for correcting the forces during monotonic compression and cyclic TC tests. The two tensile stress-strain curves for both materials, with and without side frictional forces, are compared in [figure 3](#). The difference between them is small; the maximum deviation was determined to be  $\sim 1.8\%$ .

### TENSION LU TESTS

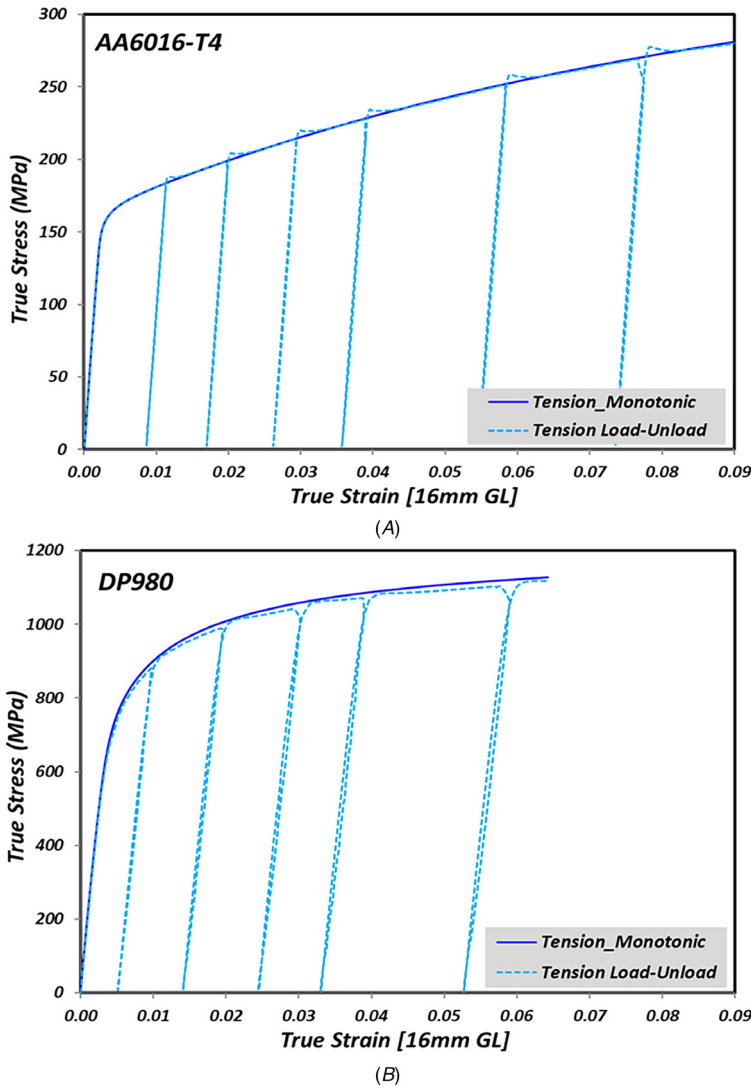
Though the tension LU tests do not require the antibuckling device, they are included here to complete the suite of mechanical tests needed for a comprehensive calibration of constitutive models for springback prediction. This test is essential for evaluating the decay in Young's modulus as a function of plastic strain. To maintain consistency, testing was carried out with the same setup: the same specimen geometry and with the DIC cameras viewing the test specimen from the side. The test program was configured as a multiloop cyclic tension test where each loading cycle was interrupted by unloading (to zero force) at a particular strain, then loading again and repeating the interruption to a greater strain. The interruption strain levels were selected to be 1%, 2%, 3%, 4%, 6%, and 8% (as permitted by the material). The resulting stress-strain curves for both the AA6016-T4 and DP980

**FIG. 3** Stress-strain curves obtained by uniaxial tension testing with and without side force for (A) AA6016-T4 and (B) DP980.



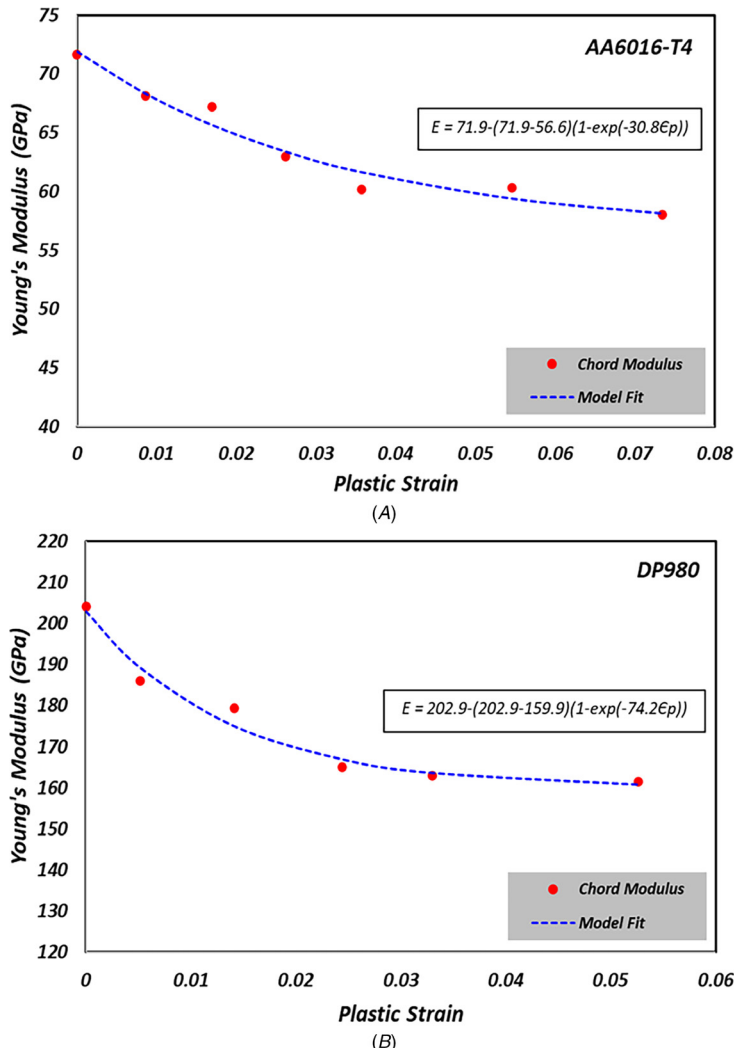
materials are shown in [figure 4](#). Greater disparity between the LU curves (higher deviation from linearity) was noted for the DP980, which increased with higher interruption strains. AA6016-T4 maintained a high level of elastic reloading curve linearity even at higher strains. The increasing nonlinearity of the reloading curves for DP980 compared to AA6016-T4 were explained by the TC testing curves shown later.

**FIG. 4** Plots showing stress-strain curve from uniaxial tension and uniaxial tension (LU) tests for (A) AA6016-T4 and (B) DP980.



By determining Young's modulus for each loading cycle and plotting that against the plastic strain level, the results shown in [figure 5](#) were obtained. A general exponential fit to capture the decay in the modulus with plastic strain has been presented in many studies in the literature;<sup>12,17-19</sup> the same model was used here to extract the fitting trend lines shown also in [figure 5](#). Both materials showed notable decay that started strong and progressively leveled out. DP980 showed clear

**FIG. 5** Plots of Young's modulus decay with plastic strain for (A) AA6016-T4 and (B) DP980.



steady-state leveling with a ~20% drop in Young's modulus; most of this decay took place after ~3% plastic strain. AA6016-T4 exhibited a similar drop in Young's modulus but after ~8% plastic strain, and that was simply due to the much higher uniform tensile ductility (~25% for AA6016-T4 compared to ~7% for DP980).

Though tension LU testing can be performed with conventional extensometry, the use of DIC enables the use of nonstandard size samples (as is the case here) to match the geometry used for all the tests for springback characterization.

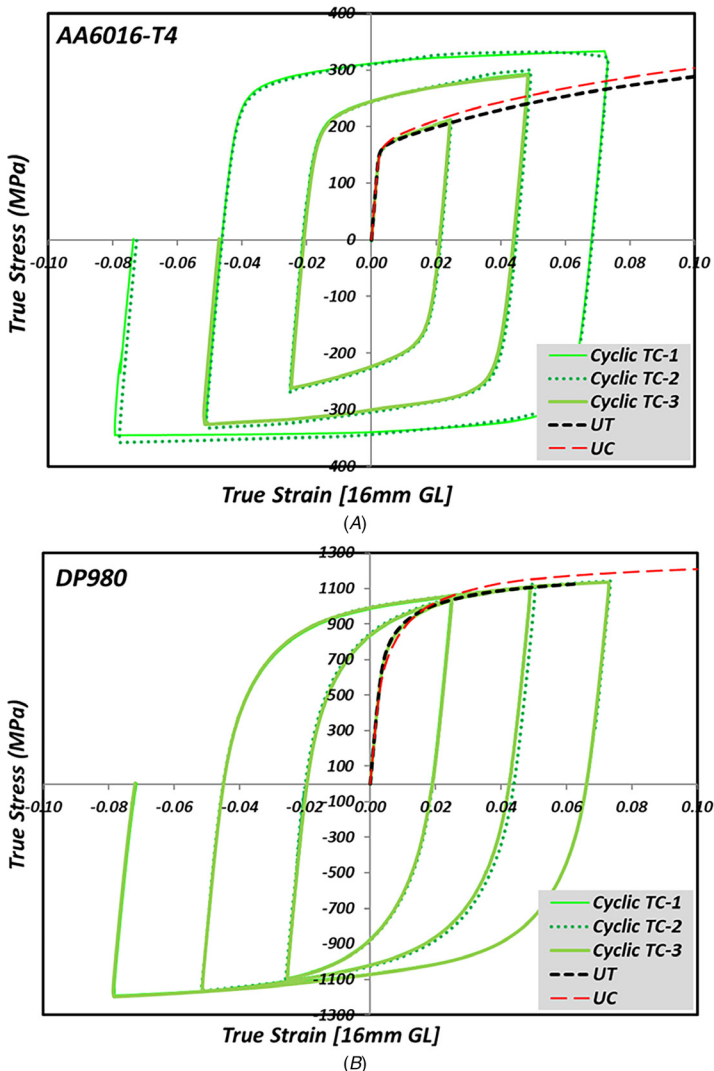
## UNIAXIAL COMPRESSION TESTS

Monotonic uniaxial compression tests were performed with the target of achieving plastic strains exceeding 10%. Tryout tests were first performed iteratively by trying increasing levels of side forces and observing the tested specimens for signs of buckling. Side forces of 2 kN and 4 kN were thus found to be satisfactory to prevent buckling in the AA6016-T4 and DP980 specimens, respectively. Actual testing then commenced, and the resulting stress-strain curves in comparison with those obtained from tension testing are shown in [figure 6](#). Note that the compression curves were intentionally flipped to the positive side of the plot to provide a direct comparison with the uniaxial tension stress-strain curves. As is clearly seen, there is a notable difference in the stress level between tension and compression, indicating asymmetry in the properties of both materials. For AA6016-T4, this asymmetry was relatively modest and took effect past the yield regime; in other words, yield strength was almost the same for tension and compression, and asymmetry was mainly noted through a modest increase in the hardening exponent and postyield flow stresses. For DP980, in addition to the higher compressive flow stress-strain curve, there was a relative rotation in the compressive curve around the yield regime when compared to the tension curve, which added complexity to the asymmetric response of this material. Such behavior is mainly driven by the complex microstructures of AHSS (the different phases of ferrite, austenite, and martensite could have different tensile and compressive properties) and by phase transformation with its dependency on the loading case (for austenite-containing AHSS).

## CYCLIC TC TESTS

The cyclic TC tests (cycles of tension followed by compression tests) were performed over three loops with progressively higher plastic strain levels of 2.5%, 5.0%, and then 7.5%. In each loop, the test specimen was first stretched to the desired strain level before reversing the direction of loading to achieve the same limit in the compressive direction and then reversing to tension again to start the next loop. Three repeats of cyclic TC tests were performed for each material. The stress-strain curves for these cyclic tests were also plotted against the earlier monotonic TC testing curves shown in [figure 6](#). The curves showed good repeatability for the first TC loop, and then the curves slightly diverged in the second and third loop. This was due to the damage in the material with increasing strain accumulation over the TC cycles. These curves showed clear differences between the two materials, particularly in the nature of their response to such cyclic loading. AA6016-T4, which showed a modest asymmetry between monotonic tension and compression, showed a complex response to cyclic loading, simply characterized by a significant increase in the overall flow stress level after each cycle. DP980, on the other hand, showed no such increase; rather, the three loops portrayed seamless progression, as if any TC testing cycle to a particular strain level was simply a part of a bigger loop that represented the global response of the material. This did not make the response of DP980 any simpler because it exhibited early reyielding for each new cycle, which

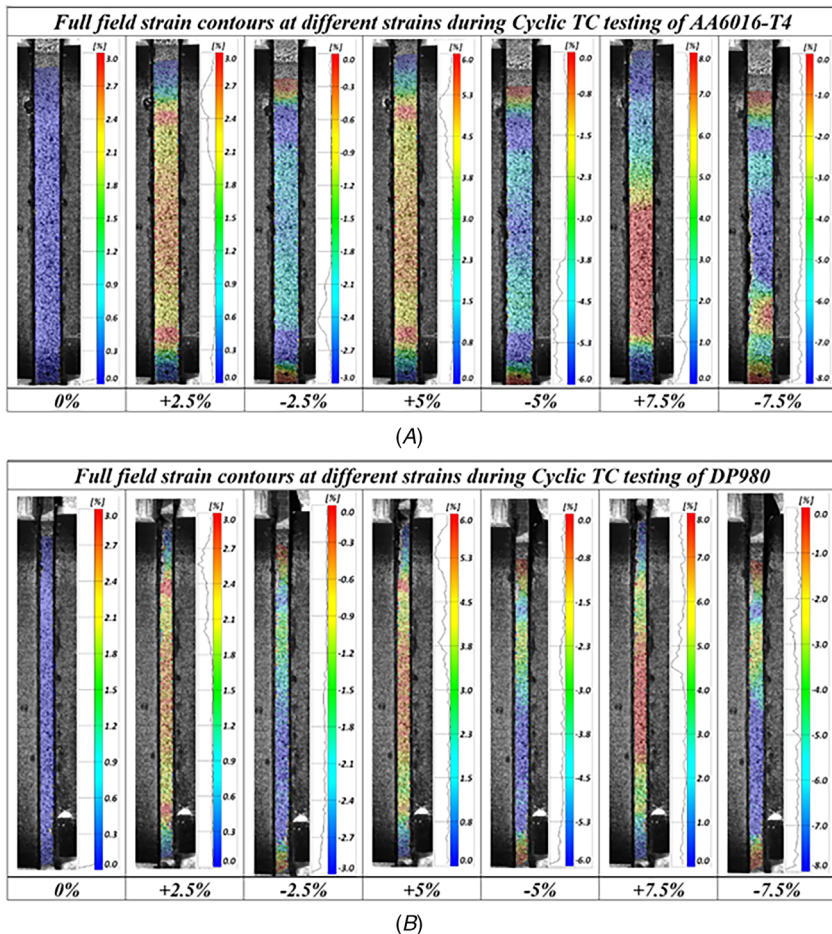
**FIG. 6** Stress-strain curves from monotonic tension tests, monotonic compression tests (flipped to positive), and three repeats of cyclic TC tests for (A) AA6016-T4 and (B) DP980.



was not the case with AA6016-T4, which showed a higher level of yielding stress for each new loading cycle! These great differences in the responses of the two materials demonstrate the importance of this particular test in revealing the complex behaviors of materials and thus enabling one to calibrate advanced springback constitutive models.

A closer look at material deformation during cyclic testing was made possible with DIC by evaluating the homogeneity of plastic deformation across the test specimen at different strain levels. **Figure 7** shows the full-field strain contour maps extracted for both materials at particular levels of plastic strain that correspond to the points of strain reversal. These maps reveal signs of deformation nonhomogeneity as early as the first point of reversal; this nonhomogeneity grows stronger with additional plastic strain accumulations and strain reversals, leading to the high levels at the end of each test. This is expected since the accumulative plastic strain imposed on the material during such cyclic tests was relatively high. When comparing the two materials, DP980 showed a greater level of nonhomogeneity throughout the cyclic

**FIG. 7** DIC-generated strain maps extracted at particular points of interest (strains) during cyclic TC testing of (A) AA6016-T4 and (B) DP980 sheet samples.



test, and that is also expected given its limited overall ductility (note that the uniform tensile ductility for this material is ~7%). These findings highlight the importance of using DIC in these tests, as it provides a mechanism for determining the appropriate parameters of TC testing for a material based on its overall ductility.

## Conclusions

In this work, characterization and modeling of springback behavior in lightweight materials were addressed from an experimental point of view by presenting a novel antibuckling device particularly designed for accurate and repeatable compression and cyclic testing, the two test types that are essential for calibrating complex spring constitutive models such as the Yoshida-Uemori Model.<sup>12</sup> In addition to the control and monitoring of side forces, self-centering, and the ability to achieve large plastic compressive strains, the antibuckling device was coupled with DIC that was run in a unique real-time mode to enable accurate strain measurements and precise load reversal during cyclic testing. The integrated setup was validated by testing AA6016-T4 aluminum and DP980 steel under different loading modes. It was shown how compression testing was successfully performed with both materials, developing compressive stress-strain curves reaching beyond 10% and enabling good evaluation of TC asymmetry in the materials. Cyclic TC tests were also successfully performed over several consecutive loops; the complexity of the test helped in revealing significant differences between the two materials in their response to alternating loading modes. In addition to the accurate strain measurements, DIC enriched these tests by revealing the levels of deformation nonhomogeneities in the tested materials and their progression with plastic strain. While this paper does not offer answers to why materials respond in different ways to complex compression or cyclic testing, as this is not its main objective, it describes advanced characterization techniques for generating the data needed for calibrating complex springback predictive models.

## References

1. M. Weiss, A. Kupke, P. Y. Manach, L. Galdos, and P. D. Hodgson, "On the Bauschinger Effect in Dual Phase Steel at High Levels of Strain," *Materials Science and Engineering A* 643 (2015): 127–136.
2. K. Han, C. J. Van Tyne, and B. S. Levy, "Bauschinger Effect Response of Automotive Sheet Steels," *Journal of Materials and Manufacturing* 114 (2005): 27–33.
3. A. Ghaei, D. E. Green, and A. Aryanpour, "Springback Simulation of Advanced High Strength Steels Considering Nonlinear Elastic Unloading–Reloading Behavior," *Materials and Design* 88 (2015): 461–470.
4. J. Mendiguren, F. Cortés, X. Gómez, and L. Galdos, "Elastic Behaviour Characterisation of TRIP 700 Steel by Means of Loading–Unloading Tests," *Materials Science and Engineering A* 634 (2015): 147–152.

5. J.-Y. Lee, F. Barlat, and M.-G. Lee, "Constitutive and Friction Modeling for Accurate Springback Analysis of Advanced High Strength Steel Sheets," *International Journal of Plasticity* 71 (2015): 113–135.
6. F. Yoshida and T. Uemori, "A Model of Large-Strain Cyclic Plasticity and Its Application to Springback Simulation," *International Journal of Mechanical Sciences* 45, no. 10 (2003): 1687–1702.
7. F. Yoshida, T. Uemori, and S. Abe, "Modeling of Large-Strain Cyclic Plasticity for Accurate Springback Simulation," *Key Engineering Materials* 340–341 (2007): 811–816.
8. L. Sun and R. H. Wagoner, "Proportional and Non-Proportional Hardening Behavior of Dual-Phase Steels," *International Journal of Plasticity* 45 (2013): 174–187.
9. B. Chongthairungruang, V. Uthaisangsuk, S. Suranunthchai, and S. Jirathearanat, "Experimental and Numerical Investigation of Springback Effect for Advanced High Strength Dual Phase Steel," *Materials and Design* 39 (2012): 318–328.
10. R. Esmaeilpour, H. Kim, T. Park, F. Pourboghrat, A. Agha, and F. Abu-Farha, "Effect of Hardening Law and Process Parameters on Finite Element Simulation of Single Point Incremental Forming (SPIF) of 7075 Aluminum Alloy Sheet," *Mechanics and Industry* 21, no. 3 (2020), <https://doi.org/10.1051/meca/2020019>
11. F. Zhou, Y. Chen, and Q. Wu, "Dependence of the Cyclic Response of Structural Steel on Loading History under Large Inelastic Strains," *Journal of Constructional Steel Research* 104 (2015): 64–73.
12. F. Yoshida, T. Uemori, and K. Fujiwara, "Elastic–Plastic Behavior of Steel Sheets under In-Plane Cyclic Tension–Compression at Large Strain," *International Journal of Plasticity* 18 (2002): 633–659.
13. R. K. Boger, R. H. Wagoner, F. Barlat, M. G. Lee, and K. Chung, "Continuous, Large Strain, Tension/Compression Testing of Sheet Material," *International Journal of Plasticity* 21, no. 12 (2005): 2319–2343.
14. T. Kuwabara, Y. Kumano, J. Ziegelheim, and I. Kuroasaki, "Tension–Compression Asymmetry of Phosphor Bronze for Electronic Parts and Its Effect on Bending Behavior," *International Journal of Plasticity* 25, no. 9 (2009): 1759–1776.
15. Q. Li, M. Jin, Z. Zou, S. Zhao, Q. Zhang, and P. Li, "Experiment Research on Tensile and Compression Cyclic Loading of Sheet Metal," *Procedia Engineering* 207 (2017): 1916–1921.
16. J. Cao, W. Lee, H. S. Cheng, M. Seniw, H. Wang, and K. Chung, "Experimental and Numerical Investigation of Combined Isotropic-Kinematic Hardening Behavior of Sheet Metals," *International Journal of Plasticity* 25, no. 5 (2009): 942–972.
17. J. Naofal, H. M. Naeini, and S. Mazdak, "Effects of Hardening Model and Variation of Elastic Modulus on Springback Prediction in Roll Forming," *Metals* 9, no. 9 (2019): 1005.
18. Z. Chen, U. Gandhi, J. Lee, and R. H. Wagoner, "Variation and Consistency of Young's Modulus in Steel," *Journal of Materials Processing Technology* 227 (2016): 227–243.
19. S. Chatti, "Modeling of the Elastic Modulus Evolution in Unloading–Reloading Stages," *International Journal of Material Forming* 6, no. 1 (2011): 93–101.